Physical and/or Chemical Compatibilization of Extruded Cellulose Nanocrystal Reinforced Polystyrene Nanocomposites

ARTICLE *in* MACROMOLECULES · JULY 2013

Impact Factor: 5.8 · DOI: 10.1021/ma4010154

2 AUTHORS:

Ning Lin
Wuhan University of Technology
18 PUBLICATIONS **624** CITATIONS
SEE PROFILE

Alain Dufresne
Grenoble Institute of Technology
312 PUBLICATIONS **15,292** CITATIONS
SEE PROFILE

Macromolecules

Article

pubs.acs.org/Macromolecules

Physical and/or Chemical Compatibilization of Extruded Cellulose Nanocrystal Reinforced Polystyrene Nanocomposites

Ning Lin and Alain Dufresne*

The International School of Paper, Print Media and Biomaterials (Pagora), Grenoble Institute of Technology (Grenoble INP), CS10065, 38402 Saint Martin d'Hères Cedex, France

Supporting Information

ABSTRACT: Impressive mechanical properties and reinforcing capability make cellulose nanocrystal (CN) a promising candidate as biomass nanofiller for the development of polymer-based nanocomposites. With the recent announcement of large-scale CN production, the use of industrial processing techniques for the preparation of CN-reinforced nanocomposites, such as extrusion, is highly required. However, low thermal stability of sulfuric acid-prepared CN limits the processing since most polymeric matrices are processed at temperatures close to 200 °C or above. It has been proved that surface adsorption of polymers on CN as compatibilizer, such as hydrophilic polyoxyethylene (PEO), can improve its thermal stability due to the shielding and wrapping of PEO. However, the weak combination between CN and PEO allows the free movement of surface polymer, which can induce the self-aggregation of CN and microphase separation in composites especially during melt processing. Using carboxylation−amidation reaction, short chains poly(ethylene glycol) (PEG) can be first grafted on the surface of the nanocrystals, and immobilize long PEO chains on modified nanocrystals through physical adsorption and entanglement. Two polymeric layers should further improve the thermal stability of CNs, and surface polymeric chains should provide significant dispersibility and compatibilization for extruded nanocomposites. Rheological analysis showed better PEO adsorption for PEG-grafted nanocrystals than pristine CN. Results from AFM and SEM revealed homogeneous dispersion and good compatibility of modified nanocrystals in PS matrix. Finally, the thermal, mechanical, and barrier properties of ensuing nanocomposites have been investigated to study the effect of physically and/or chemically modified nanocrystals.

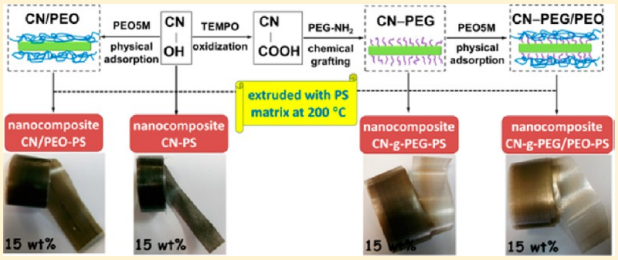

INTRODUCTION

Using controlled strong acid hydrolysis, needle-like or rod-like nanocrystals can be produced by breaking down cellulose fibers and isolating the crystalline domains. With their impressive mechanical properties, such as longitudinal modulus close to 150 GPa), high aspect ratio (10−70) and surface area (few 100 m^2/g), cellulose nanocrystals (CNs) have proven to be an ideal candidate as reinforcing bionanofiller for polymeric matrices,[1−4] since the first demonstration in 1995.[5] The mass production of CNs, which should increase upward of multiple tons per day in the future, gives a strong boost for its application in composites at industrial scale. According to the forecasting of Future Markets Inc., the production of nanocellulose (including CNs and nanofibrillated cellulose) will increase by 1000% in the next two years, and will likely increase by further 500% at least by 2017.[6]

Apart from their large-scale industrial production, the processing of CN-based nanocomposites is another crucial issue since it determines their usage properties for practical applications. Two challenges deserve more attention during the processing of nanocomposites: (1) the balance between compounding method and dispersion and (2) the compatibility of nanocrystals in polymeric matrices. Wet processing methods such as casting/evaporation, using polymer solution or polymer dispersion (latex) in liquid medium are commonly used in most studies of composites reinforced with CNs.[7,8] The main advantage of this technique is the preservation of the dispersion state of nanoparticles in the liquid medium. However, the range of available polymeric matrices is restricted, and this processing technique is both nonindustrial and noneconomic. Melting-compounding techniques, such as extrusion or injection molding, are probably the most convenient processing techniques for the industrial production of CN-based nanocomposites, because of being a green process together with large-scale production and economical availability. Extrusion is a high volume manufacturing process in which polymeric solid material is transported by a screw and melted to form a continuous profile by passing through a die. However, in most scientific studies, this conventional processing technique is infrequently employed for the preparation of CN-reinforced polymer nanocomposites. This is ascribed to the issues of low thermal stability of cellulose and inherent incompatibility between cellulose and most synthetic polymers.[9] The hydrophilic nature of cellulose causes irreversible agglomeration during drying and incompatibility with nonpolar matrices because of the formation of additional hydrogen bonds between nanoparticles.

Received: May 15, 2013
Revised: June 20, 2013
Published: July 5, 2013

   dx.doi.org/10.1021/ma4010154 | *Macromolecules* 2013, 46, 5570−5583

Moreover, because of the introduction of sulfate groups resulting from common acid hydrolysis procedure involving sulfuric acid, CNs present inferior thermal stability with degradation temperature lower than 150 °C. However, most polymeric matrices from petrochemical synthesis are melt and processed at 200 °C or above,[10] which requires higher thermal stability for CNs.

On the basis of previous studies for different nanocomposite systems reinforced with CNs, three strategies are commonly used in the processing of CN based nanocomposites by melt compounding, in order to enhance the compatibility between hydrophilic nanoparticles and hydrophobic matrices.[9] If a polar polymer is used as matrix, there is no a priori need to compatibilize the filler with the matrix material.[11,12] For nonpolar polymeric matrices, surface functionalization, such as grafting of hydrophobic moieties or chemical derivatization, can be conducted to tune the compatibility between nanoparticles and matrix.[13−17] Finally, adsorption of surfactants or macromolecules on the surface of CNs was also attempted to be used as processing aids to compatibilize cellulose nanoparticles and matrix.[18−22]

The challenge of melt processing for CN is to find the suitable treatment to both improve the thermal stability and avoid the issues of inherent incompatibility between cellulose and most polymeric matrices. In a previous work, we have demonstrated that physical adsorption of polyoxyethylene (PEO) chains on the surface of CNs can improve dispersibility and thermal stability of nanocrystals during the melt processing of low-density polyethylene (LDPE) based nanocomposites.[18] The improved thermal stability of PEO-adsorbed CNs was ascribed to a protection role of wrapped PEO chains that hides the surface sulfate groups of nanocrystals. On the other hand, it has been proved that chemical functionalization on the surface of CNs is a most effective approach to avoid irreversible agglomeration during drying, and enhance the compatibility between nanoparticles and nonpolar matrices.[13,23] In this work, surface modification through physical adsorption and/or chemical grafting was performed on cellulose nanocrystals, which produces three different types of modified nanocrystals, viz. CN/PEO, CN-*g*-PEG, and CN-*g*-PEG/PEO. Together with pristine CN, the reinforcing effect and interfacial mechanisms of four types of nanocrystals extruded with polystyrene were investigated. The PEG-covalent and PEO-noncovalent compatilization treatments affect the thermal stability of CN and rheological properties in different ways. Moreover, with the combination of strategies of grafting PEG and adsorbing PEO, novel modified nanocrystals, CN-*g*-PEG/PEO, can be prepared bearing two protective layers for CNs in order to adopt to the conditions of high temperature extrusion. It is supposed that with the common carboxylation−amidation reaction, the short grafted PEG chains (molecular weight 5000 g/mol) will evenly cover the surface of nanocrystals, which provide the first polymeric layer on nanocrystals. Because of the same chemical structure and hydrophilic property, long PEO chains (molecular weight 5×10^6 g/mol) can be tightly coupled on CN-*g*-PEG nanoparticles through entanglement and physical adsorption. Meanwhile, the immobilization of PEO5M by grafted PEG will restrict the free self-aggregation of the polymer during the processing by extrusion. As the second polymeric layer, PEO5M will play the shielding effect to surface sulfate groups of nanocrystals, and also act as a polymer compatibilizer between rigid nanofiller and polymeric matrix.

EXPERIMENTAL SECTION

Materials. Native cotton fibers were obtained from Whatman filter paper. Sodium hypochlorite (NaClO) solution was reagent grade and the available chlorine was 10−15%. Methoxypoly(ethylene glycol) amine (MPEG−NH_2) with an average molecular weight (M_w) 5000 g/mol was used in the grafting reaction with an amine loading content ≥0.17 mmol/g. Polyoxyethylene (PEO5M) with $M_w = 5 \times 10^6$ g/mol was used for the physical adsorption. Polystyrene (PS) with a density 1.047 g/mL and $M_w = 2.8 \times 10^5$ g/mol was chosen as the matrix for the processing of nanocomposites. TEMPO ($C_9H_{18}ON$, 98%), sodium bromide (NaBr), hydrochloric acid (HCl, 33%), sulfuric acid (H_2SO_4, 98%), *N*-(3-Dime-thylaminopropyl)-*N*′-ethylcarbodiimide hydrochloride (EDC), *N*-hydroxysuccinimide (NHS) and other reagents were used without further treatment. All the chemicals and materials were purchased from Sigma−Aldrich.

Extraction of Cellulose Nanocrystals from Cotton Fiber. Cellulose nanocrystals (CNs) were prepared by H_2SO_4 hydrolysis of native cotton fiber, according to our previous literature.[24] The fiber was milled with a laboratory milling device to obtain a fine particulate substance and extracted in 2 wt % NaOH solution (50.0 g of fibers for 2 L solution) for 12 h at room temperature and then filtered and rinsed with distilled water. Acid hydrolysis was performed at 45 °C with 65 wt % H_2SO_4 (preheated), for 45 min under mechanical stirring (50.0 g of fibers for 1 L acid solution). Amorphous or paracrystalline regions of cellulose were preferentially hydrolyzed, whereas crystalline regions that have higher resistance to acid attack remained intact. The suspension was diluted with ice cubes to stop the reaction and washed until neutrality by successive centrifugations at 10 000 rpm (rotation per minute) for 10 min each step, and dialyzed against distilled water for five days. After dialysis, the CN dispersion was completed by ultrasonic treatment using a Branson sonifier, and finally the released CN powder was obtained by freeze-drying.

Carboxylation of Cellulose Nanocrystals. TEMPO-mediated oxidation of CN was performed according to the procedure described in the literature.[25,26] About 20.0 g of CN (123.530 mmol anydroglucose unit AGU) was suspended in distilled water (1.5 L) and treated by ultrasonic dispersion for 10 min. TEMPO (0.579 g) and NaBr (6.353 g) were dissolved in another 100 mL distilled water and added dropwise to the nanocrystal suspension. A certain amount of 12 wt % NaClO solution was added slowly to the suspension to start the oxidizing reaction. The pH of the mixture was maintained at 10.0 by adding 0.5 M NaOH, while stirring the suspension for 4 h at room temperature. After oxidation, the reaction was quenched by adding ethanol (ca. 20 mL), and 0.5 M HCl was slowly added to the suspension to adjust the pH to 6.5−7.0. The oxidized cellulose was converted from sodium carboxylate groups (−COONa) to free carboxyl groups (−COOH). The suspension was washed thoroughly with water and then dialyzed for 24 h. Finally, by freeze-drying, the oxidized CN (OCN) powder was obtained.

Chemical Grafting of PEG5000 on Cellulose Nanocrystals. Grafting of PEG5000 onto nanocrystals was performed with the carboxylation−amidation reaction creating a covalent amide bond between a primary amine-terminated polymer and carboxylated CN by COOH−NH_2 coupling.[27] It was reported that during this reaction, the addition of NHS to EDC and amidation at neutral pH was critical to avoid the formation of the detrimental stable N-acyl urea instead of the desired amide product.[28] The grafting reaction was achieved in aqueous media with the addition of 1.2 mmol −NH_2/1 mmol −COOH. The pH of the suspension was adjusted to 7.5, and maintained throughout the reaction by adding 0.5 M HCl or 0.5 M NaOH solutions. Then, the solution containing EDC and NHS was added in the CN suspension, both 1.5 times equivalent to the carboxyl content. The reaction was carried out for 24 h at 50 °C, and finally coagulated by adding an excess of ethanol. After the reaction, the sample was dialyzed thoroughly against distilled water to remove excess reagents and free MPEG−NH_2.

Physical Adsorption of PEO5M on Pristine and Modified Nanocrystals. The weight ratio of PEO5M and nanocrystals was controlled as 35/65 during the process of physical adsorption. The typical procedure was taken from our previous paper as reference:[18] PEO solutions were prepared by adding 1.25 wt % of the polymer in distilled water. The solution was protected against light by an aluminum foil and weakly stirred at 500 rpm for 4 days at room temperature. The desired amount of pristine (CN) or grafted nanocrystal (CN-*g*-PEG)

dx.doi.org/10.1021/ma4010154 | *Macromolecules* 2013, 46, 5570−5583

aqueous suspension was added to the PEO solution. The proper amount of distilled water was then added to reach a final PEO concentration in water of 1 wt %, and the mixture was stirred for 5 h. Finally, the suspension was freeze-dried to obtain the solid products.

Preparation of Nanocomposites from Cellulose and Polystyrene by Extrusion. Nanocomposites from unmodified and modified cotton nanocrystals reinforced PS matrix were prepared by twin-screw extrusion. The lyophilizate of nanocrystals and PS pellets were introduced in the mixing chamber of a twin-screw DSM Micro 15 compounder with the following mixing condition: 200 °C at 150 rpm for 10 min. Extrusion was carried out with a slit die of 0.6 mm in width and 1 cm in length. Four kinds of nanocrystals, namely pristine nanocrystals, PEO5M-physically adsorbed nanocrystals, PEG5000-chemically grafted, and nanocrystals with both chemical PEG5000 grafting and physical PEO5M adsorption, were used to enhance the performance of PS nanocomposites, which were marked as CN−PS, CN/PEO−PS, CN-*g*-PEG−PS and CN-*g*-PEG/PEO−PS, respectively. Extruded films prepared from pure polystyrene were coded as PS−F. The compositions and labels for nanocomposites with different nanocrystal contents are shown in Table S1 (Supporting Information).

Characterization. *Fourier Transform Infrared Spectroscopy (FTIR).* Infrared spectra were recorded at room temperature on a FTIR Perkin-Elmer Spectrum One spectrometer to characterize the surface modification of nanocrystals. All freeze-dried samples were prepared as KBr pellets (1 wt % in anhydrous KBr), and analyzed using a spectral width ranging from 4000 to 400 cm^{-1} with a 2 cm^{-1} resolution and an accumulation of 32 scans.

X-ray Photoelectron Spectroscopy (XPS). The chemical modification through PEG chains grafting on the surface of nanocrystals was further analyzed by XPS. The experiments were carried out using an XR3E2 apparatus (Vacuum Generators, U.K.) equipped with an unmonochromated Mg KR X-ray source (1253.6 eV) and operated at 15 kV under a current of 20 mA. Samples were placed in an ultrahigh vacuum chamber (10^{-8} mbar) with electron collection by a hemispherical analyzer at a 90° angle. Signal decomposition was done using Spectrum NT, and the overall spectrum was shifted to ensure that the C−C/C−H contribution to the C 1s signal occurred at 285.0 kV.

Elemental Analysis. Elemental analysis was used to determine the PEG grafting efficiency on nanocrystals, which was performed at Analysis Central Service of the Centre National de la Recherche Scientifique (Vernaison, France). The carbon, oxygen, hydrogen and nitrogen elements content for both CN−COONa and CN-*g*-PEG samples were measured. PEG-grafting efficiency (GE %) was calculated according to eq 1:

$$GE\,\% \times C_{MPEG} + (1 - GE\%)C_{CN} = C_{CN-g-PEG} \quad (1)$$

where C is the relative carbon content of the sample. The precision of the measurement is considered to be 0.3% for C and H elements and 0.5% for O element.

X-ray Diffraction (XRD) Analysis. To investigate the effect of PEG grafting and PEO adsorption on cellulose nanocrystals, X-ray measurements were carried out on pristine nanocrystals, pure PEO, and modified nanocrystals. The X-ray diffraction patterns were recorded on a Philips PW 1720 X-ray generator operated at 30 kV and 20 mA with Cu Kα radiation (λ = 0.154 nm) in the range 2θ = 5−50° for samples using a fixed time mode with a step interval of 0.02°.

Atomic Force Microscopy (AFM). The morphology of CN, CN−COONa, and CN-*g*-PEG was observed with AFM. The suspensions of approximately 0.01 wt % were dispersed in water with ultrasonic dispersion for 30 min and then deposited on the mica substrate. The suspension of CN/PEO or CN-*g*-PEG/PEO complex was magnetically stirred for 1 h, and then deposited on the mica substrate. The substrate loaded with nanoparticles was imaged in tapping mode with a Nanoscope IIIa microscope from Veeco Instruments. Silicon cantilevers were used to perform the imaging at a frequency of 264−339 kHz and a typical radius of curvature of 10−15 nm.

The surface morphology of extruded nanocomposite (CN-*g*-PEG/PEO−PS-20) was investigated by AFM under QNM mode analysis. The film sample was placed on the surface of steel substrate, which was scanned at a frequency <1 Hz, and changing the rate according to the scan size. In order to observe the morphology of modified nanocrystals in extruded composites, CN-*g*-PEG/PEO−PS-20 film was dissolved in tetrahydrofuran (THF), and exchanged with acetone to remove most of PS chains. The acetone suspension containing CN-*g*-PEG/PEO nanoparticles was dropped on the mica substrate, and imaged in tapping mode.

Thermogravimetric Analysis (TGA). The contents of grafted PEG and absorbed PEO on the surface of nanocrystals were determined by thermogravimetric analysis using a thermal analyzer Perkin-Elmer TGA-6 under nitrogen flow. Freeze-dried samples of ca. 10 mg were heated from 30 to 500 °C at a heating rate of 10 °C/min.

Contact Angle Measurements. The surface hydrophilicity of cellulose before and after modification was investigated using contact angle measurement, which was performed at room temperature using a sessile drop contact angle system at Attension Theta contact angle meter. Freeze-dried nanocrystals were compacted under a pressure of 10 MPa with a KBr press to obtain samples with smooth surfaces. A small drop of water (ca. 5 μL) was deposited on the surface of the sample, while 20 pictures were taken over a period of 10 s. Attension Theta Software was used to calculate the contact angle.

Rheological Behaviors of CN or CN-g-PEG and PEO Mixtures. To investigate the capacity of CN-*g*-PEG and CN to adsorb PEO5M chains, the viscosity of various suspensions containing nanoparticles and PEO5M chains was analyzed with a rotational rheometer, Rheolyst Physica MCR-301. The cone and plate geometry, with a 50 mm diameter plate and an angle of 1°, was used. To prevent solvent evaporation during measurements, the geometry was enclosed in a solvent trap which saturates the atmosphere. The lower pan (sample chamber) was equipped with a Peltier thermoelectric device that insures a controlled temperature, fixed at 20 °C ± 0.1 °C. Viscosity of the suspension was recorded applying a flow cycle consisting in a continuously increasing shear rate ramp from 0.05 to 10 s^{-1} for 4 min. All rheological tests were performed in triplicate.

Transmittance of Visible Light. Transmittance of nanocomposite films was measured with a Shimadzu UV 2401-(PC) UV−vis spectrophotometer. The film samples were cut at 40 mm × 35 mm, and analyzed with the UV spectrophotometer within a wavelength range 200−800 nm. The transmittance spectra were acquired using air as background. The resolution of the spectrophotometer was 1.5 nm and the photometric accuracy was ±0.01 in absorption.

Scanning Electron Microscopy (SEM). The microstructure and homogeneity of extruded nanocomposites were observed using SEM on a Quanta 200 FEI device (Everhart−Thornley detector). Before observation, the samples were cryofractured and gold-coated. The cross sections were observed under an acceleration voltage of 10 kV.

Mechanical Properties. The mechanical properties of nanocomposites were investigated through dynamic mechanical analysis (DMA) measurement using a RSA3 (TA Instruments, USA) equipment working in the tensile mode. The strain amplitude was fixed at 0.05%, well below the limit of the linear viscoelastic regime. The samples were thin rectangular strips with dimensions of about 10 × 10 × 0.1 mm^3. Measurement of the storage tensile modulus ($\acute{E}$) was performed in isochronal condition (1 Hz), and the temperature varied from −60 to +150 °C at a heating rate of 5 °C/min.

Thermal Properties. The thermal behavior of nanocomposites was investigated by both differential scanning calorimetery (DSC) and thermogravimetric analysis (TGA). The glass transition temperature of nanocomposites was measured with a Perkin-Elmer DSC instrument using aluminum pans. The samples were scanned from 25 to 250 °C at a heating rate of 10 °C/min. The thermal degradation of nanocomposites was studied with a thermal analyzer Perkin-Elmer TGA-6 instrument under nitrogen flow in the temperature range from 30 to 600 °C at a heating rate of 10 °C/min.

Barrier Properties. Direct water vapor permeability (WVP) was determined from the slope of the weight gain versus time curves at 25 °C. The extruded films were sandwiched between the aluminum top (open O-ring) and bottom parts of a specifically designed permeability cell with screws containing 5.0 g of anhydrous calcium chloride ($CaCl_2$) to generate 0% relative humidity (RH). A Viton

dx.doi.org/10.1021/ma4010154 | Macromolecules 2013, 46, 5570−5583

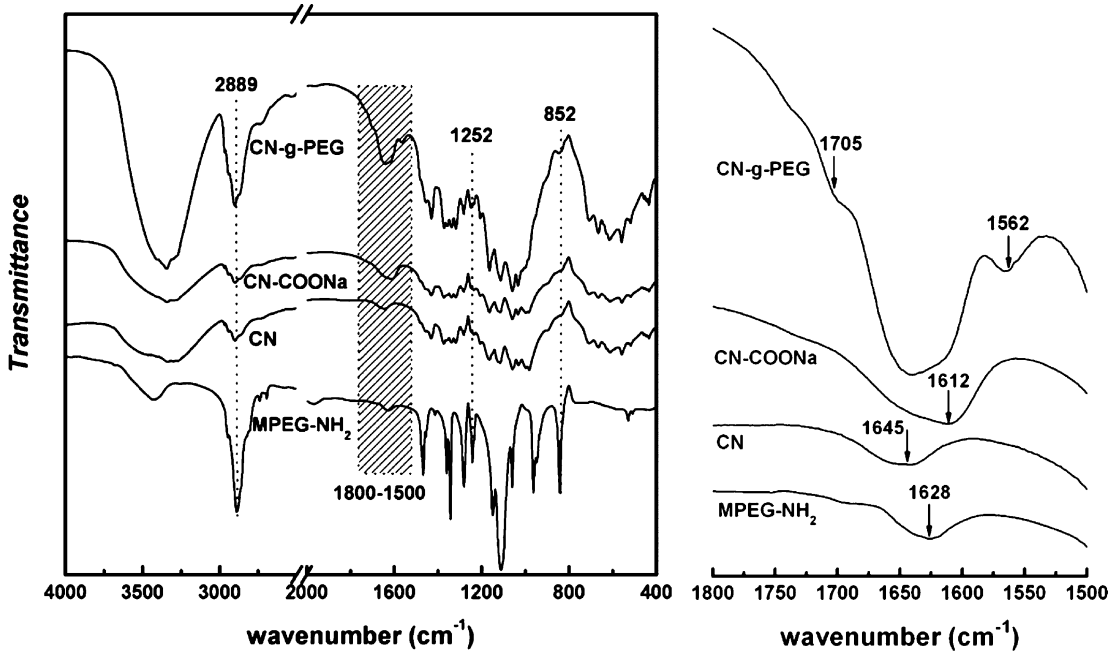

Figure 1. FTIR spectra for MPEG−NH_2, CN, CN−COONa, and CN-*g*-PEG.

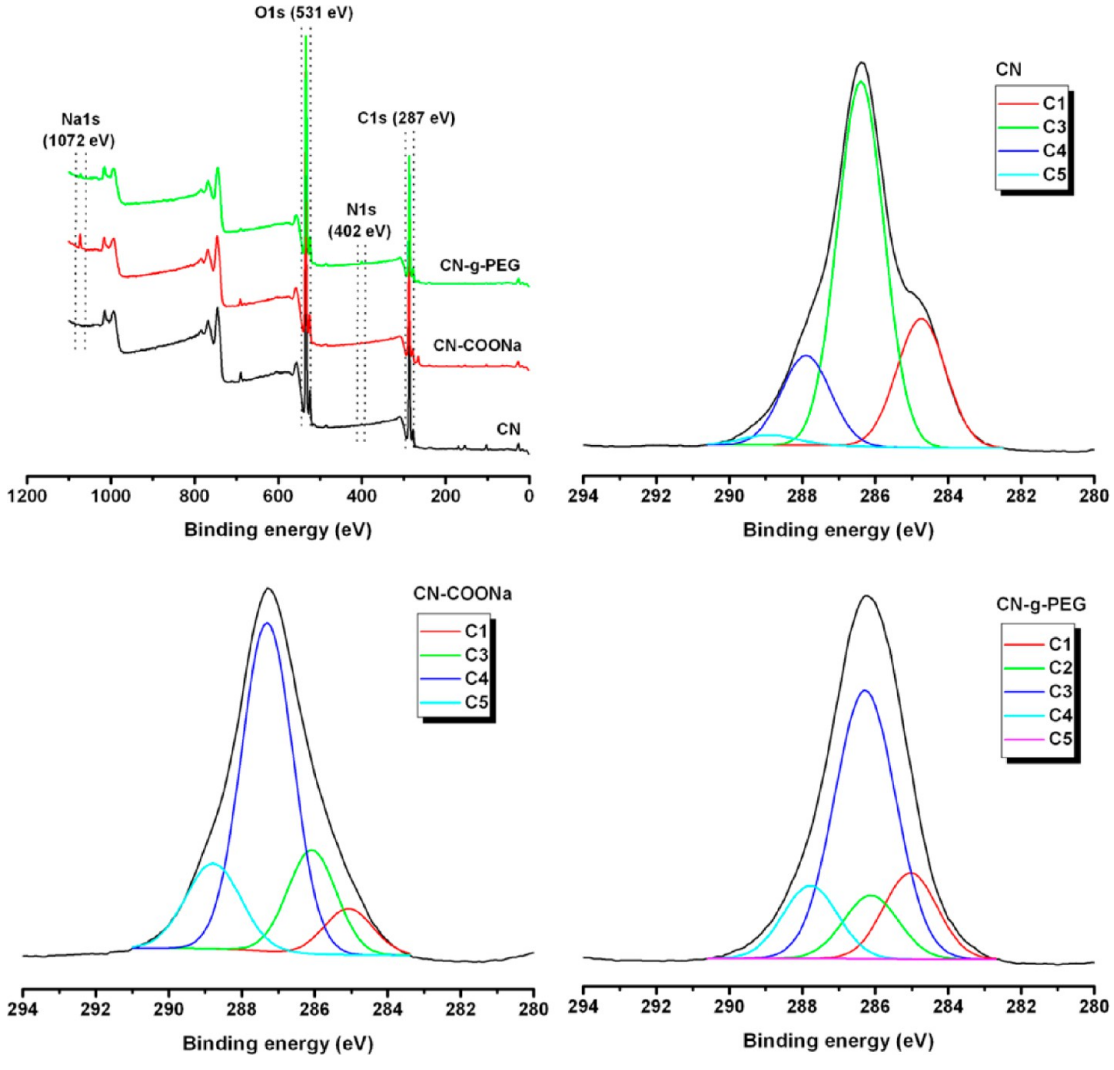

Figure 2. General XPS spectra for CN, CN−COONa, and CN-*g*-PEG with signal assignments; XPS decomposition of the C 1s signal into its constituent contributions for CN, CN−COONa, and CN-*g*-PEG.

dx.doi.org/10.1021/ma4010154 | *Macromolecules* 2013, 46, 5570−5583

rubber O-ring was placed between the nanocomposite film and the bottom part of the cell to enhance sealability. Then, the cells were placed in the desired environment of 50% RH at 25 °C, and the water vapor weight gain through the film was monitored as a function of time. Water weight gain was calculated as the total cell weight gain minus the gain through the sealing. All the tests were performed in duplicate, and WVP value of each nanocomposite was calculated as the average according to eq 2:

$$\mathrm{WVP(g/m\cdot S\cdot Pa)} = \frac{\Delta me}{A\Delta t\Delta P} \quad (2)$$

where Δm is the mass increase (g) of the $CaCl_2$ sample, A is the area of the film (4×10^{-4} m^2), and Δt is the exposure time in the chamber. The thickness of the film is e and ΔP (1425.36 Pa) is the partial water vapor pressure difference across the film specimen corresponding to 50% RH at 25 °C.

RESULTS AND DISCUSSION

Surface Modification and Properties of Cellulose Nanocrystals. Chemical grafting of PEG chains on the surface of cellulose nanocrystals was investigated by FTIR spectra, as shown in Figure 1. Although the peaks for CN-*g*-PEG located at 2889, 1252, and 852 cm^{-1} were overlapped with cellulose component, the increase of intensity for these peaks still can be observed by comparing the spectra for CN-*g*-PEG and CN, which was ascribed to the coupling of PEG on nanocrystals. More evident changes for modified nanocrystals were presented in the spectrum range 1800−1500 cm^{-1}. Two additional peaks appeared at 1562 and 1705 cm^{-1} on the spectrum for PEG-grafted nanocrystals, corresponding to the stretching vibrations of amide groups and carboxyl groups, respectively.[27] These characteristic peaks were not visible on the spectrum for pure MPEG−NH_2. Moreover, it should be pointed out that the appearance of a stretching band at 1612 cm^{-1} on the spectrum for carboxylated (ungrafted) nanocrystals (CN−COONa) was assigned to salt forms of carboxylic acid, as reported in our previous work.[24]

Further verification and grafting efficiency for CN surface modification were realized by XPS and elemental analysis. As shown in Figure 2, on the general XPS spectra, there were new signals corresponding to nitrogen (N 1s: 402 eV) and sodium (Na 1s: 1072 eV) assigned to the surface chemistry of CN-*g*-PEG and CN−COONa samples in comparison with CN. On the other hand, high resolution C 1s spectra were resolved into several components (Table S2 in Supporting Information) which were assigned to C−C/C−H (285 eV, the binding energy scale was changed according to this value as starting position), C−N (286.2 eV), C−O (286.5 eV), O−C−O/C═O (288.05 eV), O−C═O (289.0 eV). It was clear that in comparison with pristine CN and CN−COONa samples, only the spectrum of CN-*g*-PEG showed evident C−N peak, which corresponded to the covalent coupling from carbodiimide grafting reaction. Furthermore, from the ratio change of different compositions of carbon signal, the proportion of C4 (C═O) and C5 (O−C═O) for CN−COONa sample increased obviously, which indicated the adequate surface modification of nanocrystals from hydroxyl groups to carboxyl groups. The grafting efficiency (GE %) of PEG chains for CN-*g*-PEG sample was determined from the results of elemental analysis reported in Table S2 (Supporting Information). Because of only surface carboxylation of cellulose nanocrystals, pristine CN and CN−COONa samples have similar chemical compositions, which exhibited small change of element contents (C, O, and H) for carboxyl nanocrystals. However, the significant difference in the elemental composition for pure cellulose and poly(ethylene glycol) provides the possibility to compare the elemental change before and after chemical grafting. The nitrogen content (0.43) for CN-*g*-PEG samples provided the critical result to prove the successful grafting reaction. Considering instrumental error and adsorption of moisture for hydrophilic materials during the delivery and manipulation, the values of grafting efficiency were confirmed mainly based on the data from carbon element, and calculated according to eq 1. as 21.77 wt %, which was nearly in agreement with previous report (ca. 20−30 wt %).[27]

The changes in nanocrystal crystallinity induced by chemical grafting and/or physical adsorption were investigated by XRD analysis (Figure 3). Pure MPEG−NH_2 and PEO5M showed

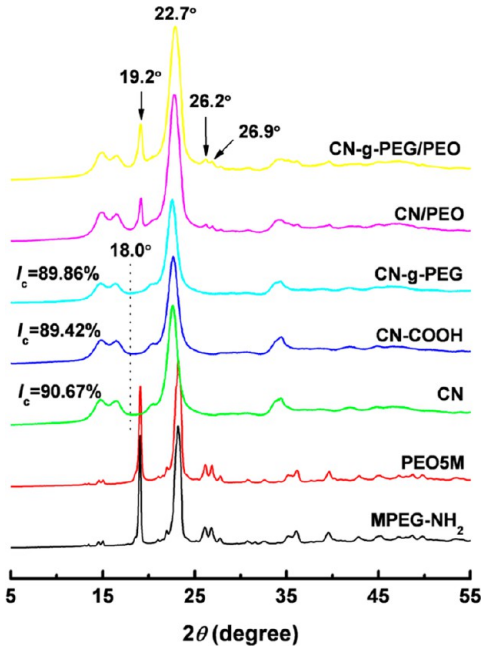

Figure 3. X-ray diffraction patterns for pure MPEG−NH_2, PEO5M, CN; CN−COONa, CN-*g*-PEG; and CN-*g*-PEG/PEO, CN/PEO complexes.

the same crystalline features at 2θ = 19.2°, 22.5°−23.5°. However, these characteristic peaks cannot be observed on the pattern for CN-*g*-PEG, which was attributed to the amorphous state of grafted PEG chains, and limited surface crystallization from relatively short chain length.[27,29] The quite similar patterns for pristine CN, carboxylated CN−COONa, and grafted CN-*g*-PEG indicated the original integrity of cellulose crystal after chemical modification. In fact, from the calculation according to the Segal method,[30] the crystallinity index (I_c) of cellulose was about 90.67% for CN, 89.42% for CN−COONa, and 89.86% for CN-*g*-PEG. The main peak at 2θ = 22.5° (002) for cellulose shifted to 22.7°, and became broader. Meanwhile, new crystalline peaks at 2θ = 19.2°, 26.2°, and 26.9° ascribed to PEG and/or PEO chains appeared on the patterns of these two complexes.

The morphology of pristine CN, chemically modified nanocrystals (CN−COONa and CN-*g*-PEG), and physically adsorbed complexes (CN/PEO and CN-*g*-PEG/PEO) were observed using AFM as shown in Figure 4. Pristine CN presented a typical rod-like morphology with a length of 100−300 nm and a diameter of 5−20 nm (image A). After carboxylation, CN−COONa also maintained the rod-like

dx.doi.org/10.1021/ma4010154 | Macromolecules 2013, 46, 5570−5583

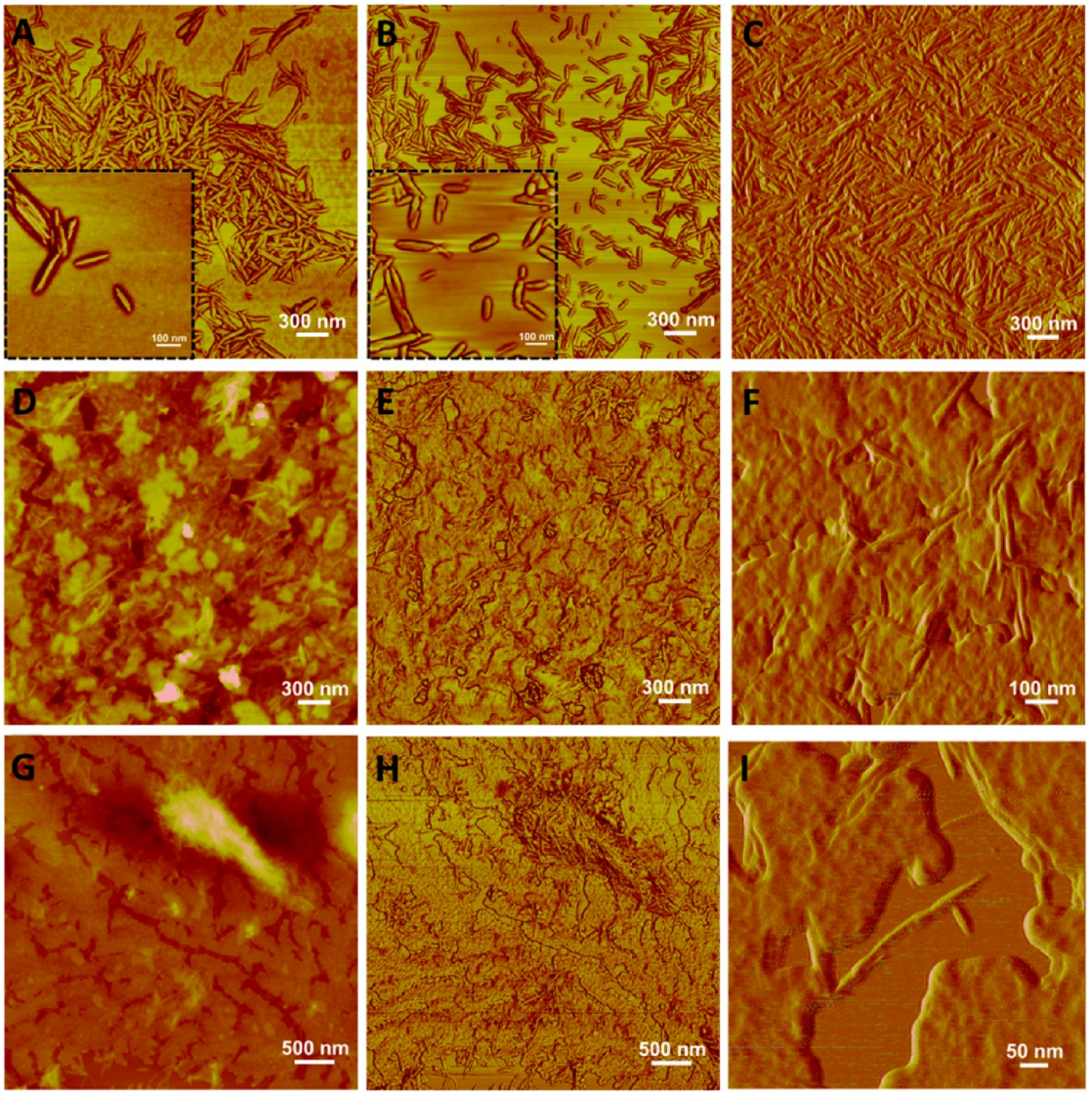

Figure 4. AFM images for (A) CN, (B) CN−COONa, (C) CN-*g*-PEG, (D−F) CN-*g*-PEG/PEO, and (G−I) CN/PEO.

shape, and exhibited improved dispersibility in water (image B). Because of the electrostatic repulsion between grafted chains, CN-*g*-PEG showed much better dispersibility in water than unmodified nanocrystals (image C). By comparing the images for CN-*g*-PEG/PEO and CN/PEO, some interesting observations can be found. Because of surface adsorption of high molecular weight polymer (PEO5M), these two samples tended to form a membrane on the substrate. For the complex with homogeneous adsorption and dispersion of nanoparticles, the images for the membrane are regular and ordered, just as CN-*g*-PEG/PEO in images D and E. Further observation at higher resolution (image F) indicated that nanocrystals embedded in the complex with the surrounding PEG and PEO chains. However, for the CN/PEO complex, a serious aggregation appeared (images G and H), which may include aggregated nanoparticles and/or PEO. In any case, the adsorption of PEO on pristine CN showed irregular arrangement and ineffective organization. With observation at higher resolution, it even appeared some isolated nanocrystals without any immobilization of PEO chain (image I). It was supposed that CN-*g*-PEG can absorb PEO more efficiently, and regularly arrange these polymeric chains on the surface of CN-*g*-PEG;

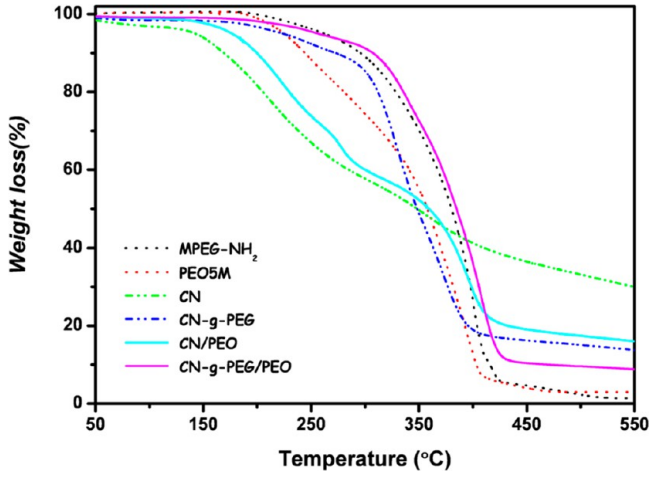

Figure 5. TGA thermograms for pure MPEG−NH_2, PEO5M; pristine CN, grafted CN-*g*-PEG; and CN/PEO and CN-*g*-PEG/PEO complexes.

while pristine CN can only immobilize few amount of PEO, and many more polymeric chains should be free and away from

dx.doi.org/10.1021/ma4010154 | *Macromolecules* 2013, 46, 5570−5583

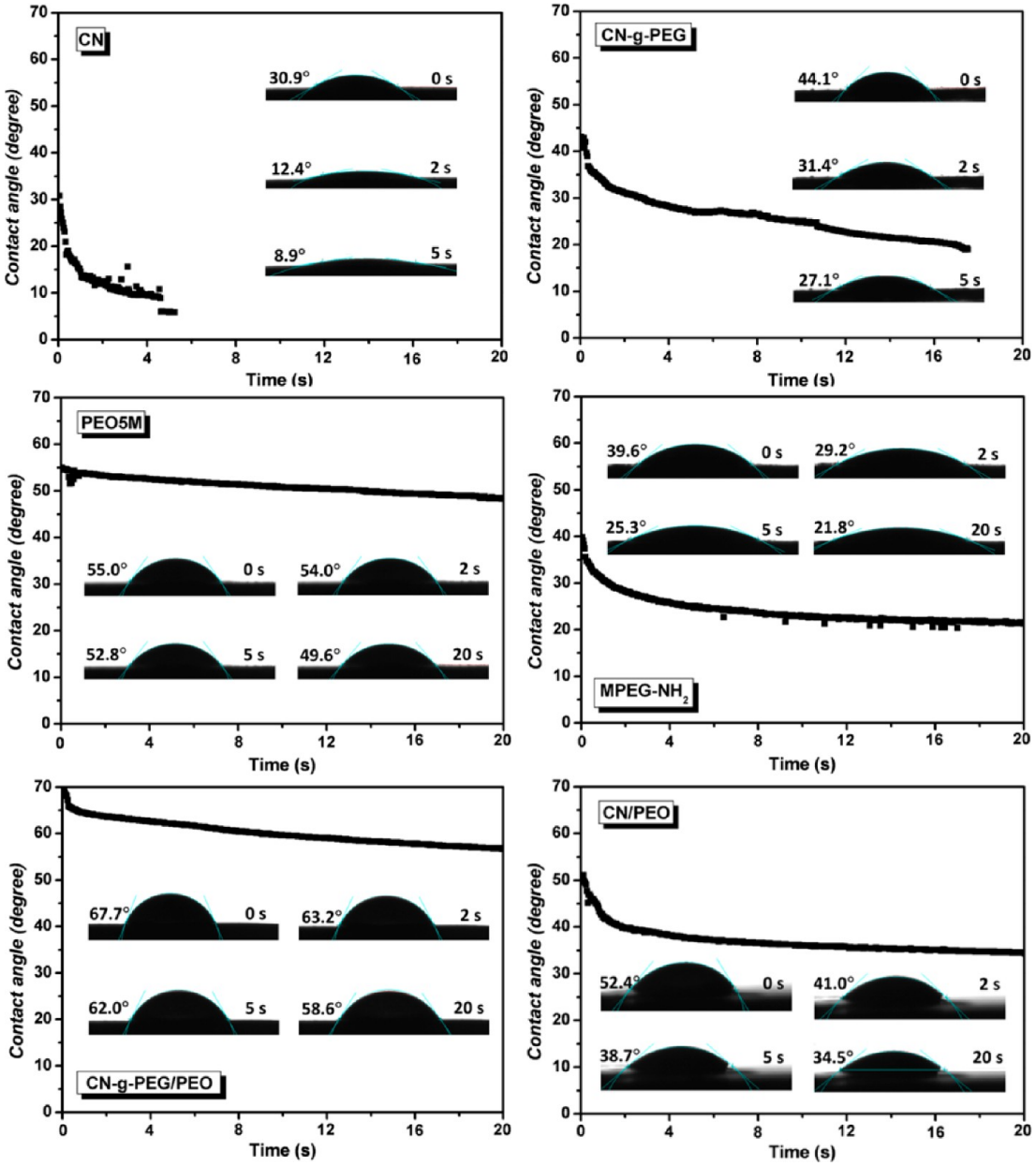

Figure 6. Time-dependence of contact angle for one drop of water on sheet samples, and inserted photographs for the water drop on the sheet samples after 0, 2, 5, and 20 s. (Zero time is the moment of drop deposition.)

nanoparticles. Three additional experiments, TGA for thermal properties, contact angle measurement for surface hydrophilicity, and rheological behavior of the suspensions, were performed to support this supposition.

The thermal degradation of nanocrystals before and after chemical and/or physical modification is shown in Figure 5. It is known that the presence of sulfate groups on the surface of CN induces the reduction of its thermal stability. This reduction of thermal stability depends on the density of sulfate groups and then hydrolysis conditions. Neat H_2SO_4-prepared CN starts to degrade from 150 °C (Figure 5). When PEO is adsorbed on the surface of CN, the degradation temperature of CN/PEO was slightly improved to about 160 °C. Moreover, a two-step degradation process was observed for CN/PEO. The low temperature process starting from 160 °C is most probably ascribed to the degradation of cellulose, and the high temperature process starting at 300 °C is possibly attributed to the degradation of PEO. These results revealed the limited adsorption and weak interaction between pristine nanocrystals and PEO chains. With the surface grafting of PEG, CN-*g*-PEG showed a significant enhancement of the degradation temperature, which can be attributed to the uniform shield of sulfate groups induced by the coating with the grafted PEG layer. Regarding the CN-*g*-PEG/PEO complex, the thermal degradation was further improved, which presented only 5% weight loss at the temperature of 320 °C. This improvement can be explained by the covalent protection provided by the PEG layer, and the close connection and interaction between PEG and PEO chains.

The influence of chemical grafting and physical adsorption on the surface hydrophilicity of cellulosic nanoparticles was further investigated by contact angle measurement, as shown in Figure 6. The contact angle of the water drop for pristine CN decreased sharply with spreading in 5 s, which resulted from the

dx.doi.org/10.1021/ma4010154 | *Macromolecules* 2013, 46, 5570−5583

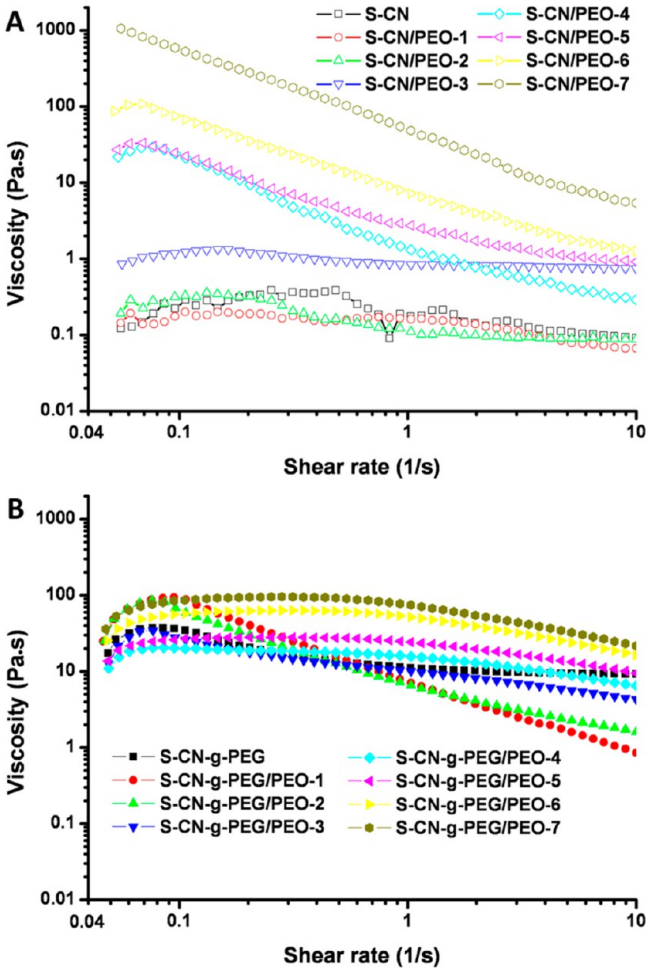

Figure 7. Viscosity vs shear rate for suspensions: (A) PEO5M-adsorbed CN; (B) PEO5M-adsorbed CN-*g*-PEG with a continuously increase of the shear rate from 0.05 to 10 s^{-1} for 4 min at 20 °C. The labels in figure correspond to the gradual increase of PEO5M content in suspensions as shown in Table S3 (Supporting Information).

swelling property of cellulose by water.[31] For PEG-grafted nanocrystals (CN-*g*-PEG), the contact angle kept a similar reduction with time as CN due to the gradual spread of the drop on the PEG layer. In spite of similar chemical structure, the dynamic contact angle for pure PEO5M remained roughly constant around 50°, whereas the one for pure MPEG−NH_2 gradually decreased from 39.6° to 21.8° over 20 s, which indicated the significant effect of the molecular weight of poly(ethylene glycol) polymers to surface hydrophilicity. Interestingly, the value of the contact angle for CN-*g*-PEG/PEO (67.7°) was even higher than that of pure PEO5M, which reflected the tight combination resulting from entanglements between PEG and PEO chains. On the contrary, because of the weak immobilization and uneven coverage of PEO on pristine nanocrystals (CN/PEO), the water drop was prone to penetrate through the PEO layer and directly contact the surface of cellulose, which induced the obvious reduction of the contact angle. The difference and change of surface hydrophilicy together with the thermal degradation behavior for CN-*g*-PEG/PEO and CN/PEO complexes indicated the role of grafted PEG chains helping the immobilization of PEO chains.

Direct study of the capability of pristine CN and CN-*g*-PEG to absorb PEO polymeric chains can be investigated by studying the rheological behavior of nanocrystal suspensions in the presence of PEO. For this study, suspensions with a constant nanocrystal concentration and gradual increase of PEO content in Table S3 (Supporting Information) were prepared and their viscosity vs shear rate was determined. As shown in Figure 7A, the suspensions with low PEO content (S-CN/PEO-1 and S-CN/PEO-2) presented a similar behavior as the neat CN suspension, which indicated the capability of surface adsorbing 0.15−0.30 g of PEO for 1.0 g of pristine CN. This result was nearly in accordance with our previous report of optimal ratio for PEO-adsorbed CN (20 wt % PEO/80 wt % CN).[18] The addition of higher PEO content in the CN suspension releases free polymer chains, and induced the increase of the viscosity. For PEG-grafted nanocrystals (CN-*g*-PEG), a maximum of 0.60 g of PEO polymer (S-CN-*g*-PEG/PEO-5) can be adsorbed. Grafted

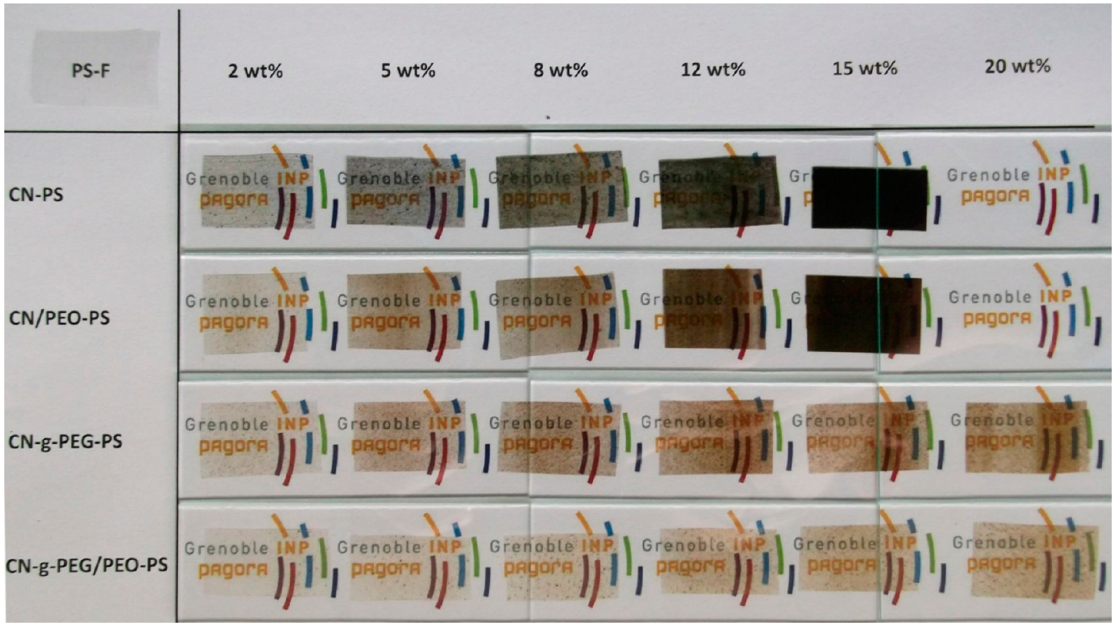

Figure 8. Pictures for extruded nanocomposites filled with pristine CN, CN/PEO, CN-*g*-PEG, and CN-*g*-PEG/PEO nanohybrids.

dx.doi.org/10.1021/ma4010154 | *Macromolecules* 2013, 46, 5570−5583

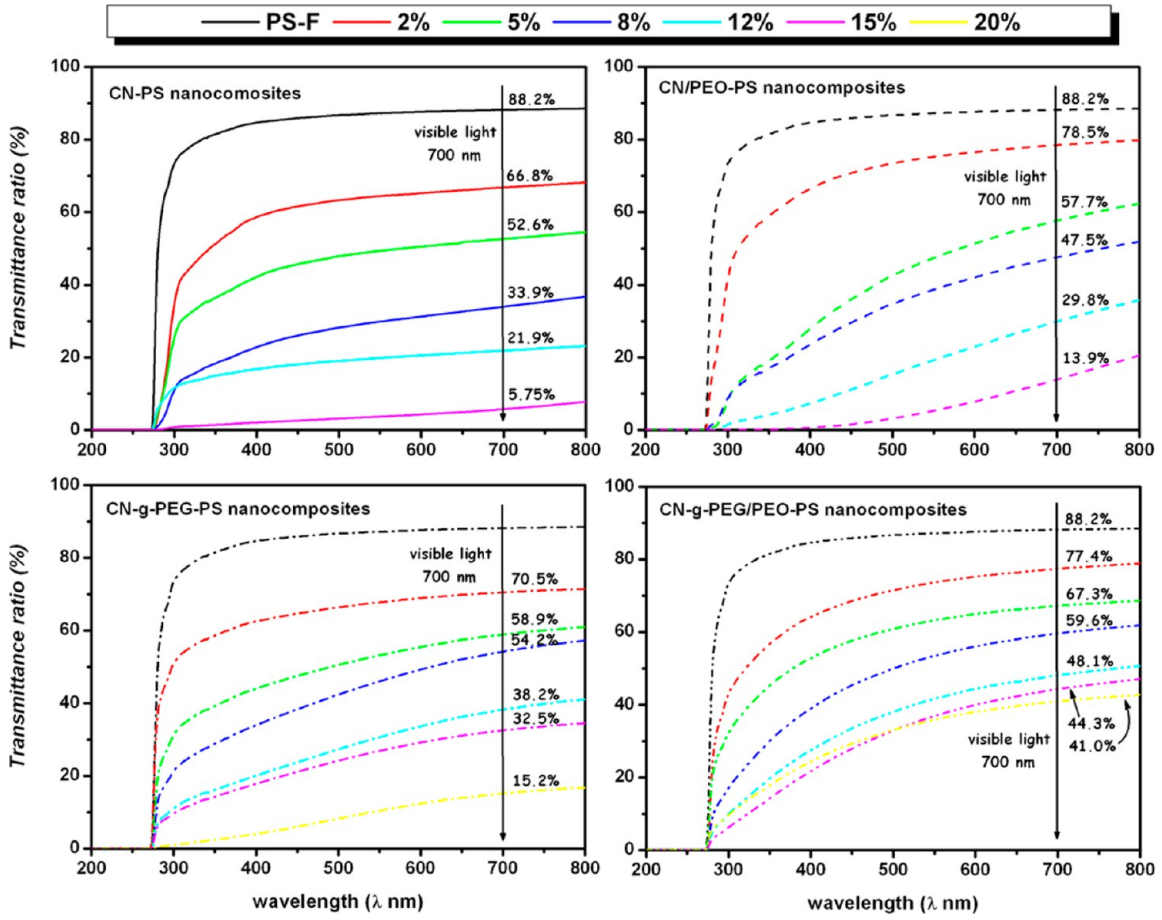

Figure 9. UV transmittance spectra for CN−PS, CN/PEO−PS, CN-*g*-PEG−PS, and CN-*g*-PEG/PEO−PS nanocomposites.

nanocrystals display roughly a two times higher PEO-adsorbing capability than pristine CN (Figure 7B). The comparison of the rheological behavior between PEO-adsorbed CN-*g*-PEG and CN suspension proved a more effective adsorption and immobilization of PEO chains on nanocrystals probably because of entanglements between grafted PEG chains and PEO chains. It is worth noting that in this work the ratio of nanocrystals and absorbed PEO5M was controlled as 65/35 (w/w) to ensure the adsorption of all the PEO on CN-*g*-PEG, which was close to the capability of surface adsorbing 0.54 g of PEO for 1.0 g of nanocrystals.

Structure and Properties of Extruded Nanocomposites. Pristine nanocrystals as well as physically and/or chemically modified nanocrystals, viz. CN, CN/PEO, CN-*g*-PEG, and CN-*g*-PEG/PEO, were extruded with a PS matrix for the preparation of nanocomposites. The microstructure and interfacial mechanisms were investigated and discussed on the basis of the properties and comparison of the different series of extruded nanocomposites. First, Figure 8 shows the appearance of extruded nanocomposites with four nanohybrids. The addition of pristine CN progressively darkens the nanocomposites extruded at 200 °C. Despite the homogeneous dispersion of dark dots, the color of nanocomposites gradually darkened with the increase of CN content, which was ascribed to the low thermal degradation temperature of cellulose and further reduction of thermal stability from sulfate groups during the extraction of nanocrystals. Especially, the nanocomposite with 15 wt % pristine CN (CN−PS-15) was completely dark and opaque. Regarding the incorporation of PEO5M-adsorbed nanocrystals (CN/PEO), although the darkness of nanocomposites containing low nanofiller content was less pronounced, a serious degradation of cellulose still occurred for extruded nanocomposites with higher CN/PEO contents (12 and 15 wt %). It was reported that the adsorbed polymeric PEO layer can play an effect of coating and shielding for surface sulfate groups on nanocrystals.[18] However, it is worth noting that in this previous work extrusion was performed at 160 °C using low density polyethylene as matrix. In present work, extrusion was carried out at 200 °C. Moreover, when adding higher PEO-adsorbed nanocrystal contents, the physical protection provided by the PEO layer may be lost because of the tendency to aggregation of hydrophilic PEO in hydrophobic PS matrix. The problem of lower thermal stability of CNs can be improved considerably by surface chemical modification. As shown in Figure 8, CN-*g*-PEG−PS based nanocomposites exhibited transparent or translucent appearance, even introducing high nanofiller contents (20 wt %), which can be attributed to the covalent and close conjunction between PEG chains and nanocrystal. However, due to the shortness of PEG chains, the whole surface of the nanocrystal may not be fully covered by grafted chains, which caused the inhomogeneous appearance of extruded nanocomposites. The most promising materials were nanocomposites reinforced with nanocrystals subjected to both physical and chemical modification, i.e., CN-*g*-PEG/PEO−PS. All extruded nanocomposites were transparent, and presented homogeneous dispersion of the nanofiller. In comparison with CN/PEO and CN-*g*-PEG, both a covalently grafted-PEG layer, together with homogeneous PEO-adsorbed

dx.doi.org/10.1021/ma4010154 | *Macromolecules* 2013, 46, 5570−5583

layer resulting from tight entanglement and attraction between compatible PEG and PEO chains were present. The immobilization of long PEO chains on nanocrystals with grafted PEG chains restricted the tendency of PEO self-aggregation, and promoted the protective effects from two polymeric layers.

The light transmittance ratio of extruded nanocomposites was measured using UV spectrophotometer, as shown in Figure 9. It shows that the addition of nanoparticles in PS matrix induced a decrease of light transmittance, especially for composites containing high filler contents. However, this effect was completely different for the four nanohybrids. The introduction of CN or CN/PEO caused a sharp decrease of the light transmittance for PS based nanocomposite films, which presented such low transmittance ratios as 5.75% and 13.9% (maximum visible light at 700 nm) for CN−PS-15 and CN/PEO-15 nanocomposites. For nanocomposites loaded with chemically modified nanocrystals, such as CN-*g*-PEG−PS-15, the transmittance ratio at light wavelength of 700 nm was improved to 32.5%. However, with the addition of higher CN-*g*-PEG contents (20 wt %), the transmittance ratio of the nanocomposite decreased sharply. The most interesting result was obtained for CN-*g*-PEG/PEO−PS nanocomposites. Despite the gradual reduction of the transmittance ratio, when increasing the nanofiller content, all extruded nanocomposites maintained the high transmittance to some extent, such as all series materials behaving a transmittance ratio of visible light >40%.

The surface of CN-*g*-PEG/PEO−PS-20 nanocomposite and morphology of nanohybrids inside the extruded composite were observed by AFM with QNM and Tapping modes. As shown in Figure 10A, the surface image of CN-*g*-PEG/PEO−PS-20 nanocomposite exhibited uniform and regular aspect, which should indicate good compatibility and miscibility of all components in the matrix. The nanoparticles were extracted from the extruded composite by dissolution of the material in THF and exchange to acetone for the removal of the PS matrix. The morphology of the extracted nanoparticles was observed (Figure 10B). It was observed that hydrophilic CN-*g*-PEG/PEO complexes aggregated upon drying, but kept their original rod-like shape and dimensions.

Further investigation of the microstructure of extruded nanocomposites was performed by observing their cryofractured cross-section morphology by SEM. As shown in Figure 11, compared to neat PS−F (image A), some nanoscaled dark dots were observed for CN−PS-2 nanocomposite (image B). Much more dots appeared in the cross-section morphology of CN−PS-15 nanocomposite (as indicated by yellow arrow and circle in image C), which were attributed to the carbonization and degradation of nanocrystals during extrusion. For PEO-adsorbed nanocrystals, due to the coverage and filling of PEO chains on the surface of nanocrystals, no more dark dots were observed as shown for CN/PEO−PS-2 and CN/PEO−PS-15 (images D and E). However, serious inhomogeneity and microphase separation existed in these nanocomposites, especially for high CN/PEO contents, such as the evident hole in the cross-section of CN/PEO-15 (as indicated by red arrow in image E). Regarding the nanocomposites filled with CN-*g*-PEG (images F and G) and CN-*g*-PEG/PEO (images H and I), a similar cross-section morphology as the one observed for PS−F was reported, which indicated the good dispersion level and miscibility of these two nanofillers within the matrix. It is worth noting that although having the same PEO content, no microphase separation was observed for

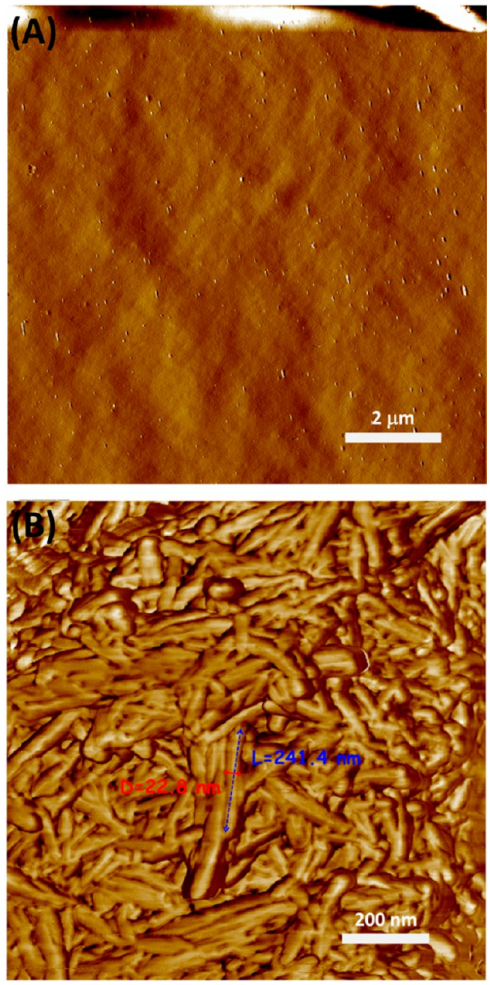

Figure 10. AFM images for extruded nanocomposite CN-*g*-PEG/PEO−PS-20 (A) and suspension of CN-*g*-PEG/PEO−PS-20 nanocomposite dissolved in THF and exchanged with acetone (B).

CN-*g*-PEG/PEO−PS-15 (image I) contrarily to CN/PEO−PS-15 (image E). It is ascribed to favorable interactions between adsorbed PEO and grafted PS chains in the nanocomposite.

The thermal properties of extruded nanocomposites, such as glass transition temperature (T_g) of polystyrene component, melting temperature (T_m) of PEO component, and degradation temperature (T_d), were analyzed using DSC and TGA. As shown in DSC thermograms in Figure 12, the introduction of pristine CN or CN/PEO in PS matrix caused a slightly gradual decrease of T_g-PS. It is ascribed to inherent incompatibility between cellulose and polystyrene, and ensuing weak interfacial interactions between the nanofiller and the matrix. It indicates that the simple addition of hydrophilic CN and physical PEO adsorption on nanocrystals cannot allow homogeneous dispersion in the hydrophobic PS matrix. On the contrary, for CN-*g*-PEG and CN-*g*-PEG/PEO reinforced nanocomposites T_g-PS remains stable or slightly increases upon nanofiller addition. It is an indication that chemical grafting improves the compatibility of the nanoparticles with the PS matrix. Furthermore, a melting endotherm was visible for highly filled PEO-adsorbed CN (CN/PEO and CN-*g*-PEG/PEO) nanocomposites. It is obviously ascribed to the melting point of the PEO phase (T_m-PEO). The same PEO was used for the two series of extruded nanocomposites, but it appears for lower CN content for PEG-grafted nanoparticles. The chemical grafting

dx.doi.org/10.1021/ma4010154 | *Macromolecules* 2013, 46, 5570−5583

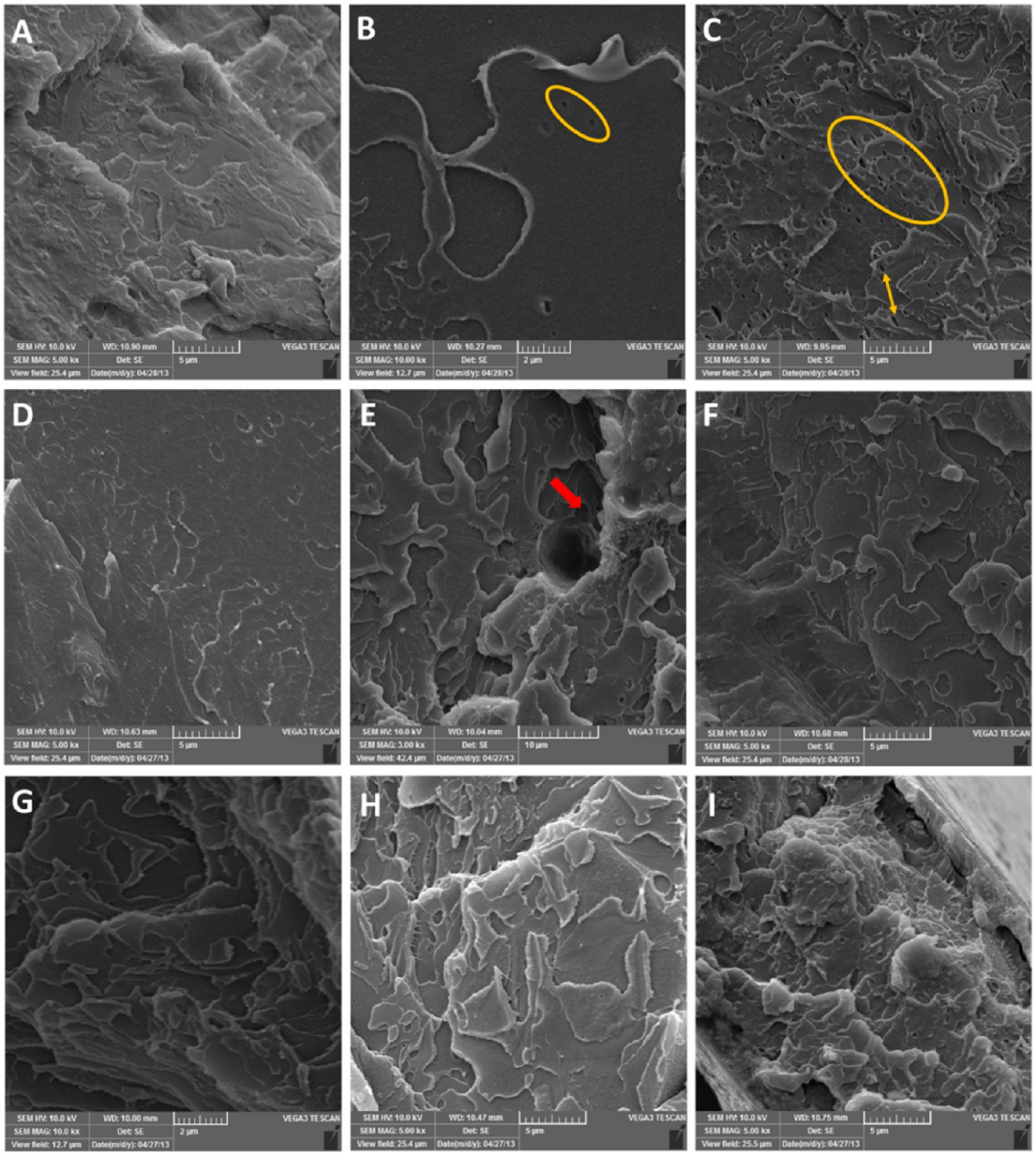

Figure 11. SEM images of the cross-section for extruded PS nanocomposites with low (2 wt %) and high nanohybrid content (15 wt %): (A) PS−F; (B) CN−PS-2, (C) CN−PS-15; (D) CN/PEO−PS-2; (E) CN/PEO−PS-15; (F) CN-*g*-PEG−PS-2; (G) CN-*g*-PEG−PS-15; (H)CN-*g*-PEG/PEO−PS-2; (I) CN-*g*-PEG/PEO−PS-15.

improves the ability of adsorbed PEO chains to crystallize possibly because of cocrystallization between grafted and adsorbed polymeric chains. Moreover, T_m-PEO was located around 55−56 °C for CN/PEO−PS and slightly higher than 60 °C for CN-*g*-PEG/PEO−PS. This significant increase of T_m-PEO for CN-*g*-PEG/PEO−PS nanocomposites reflects bigger crystal size for PEO.

TGA experiments were performed to evaluate the thermal stability for extruded nanocomposites loaded with low (2 wt %), moderate (8 wt %), and high (15 wt %) nanofiller contents, as shown in Figure 13. Compared to neat PS−F material, the initial degradation temperature (T_{d1}) corresponding to 5% weight loss for all extruded nanocomposites was increased; especially for CN/PEO−PS-15 and CN-*g*-PEG/PEO−PS-15 nanocomposites for which the increment in T_{d1} value was higher than 30 °C. This effect is probably ascribed to favorable interactions between adsorbed PEO chains and PS matrix chains. Complete thermal degradation of polystyrene occurred around 415 °C, as shown in the thermogram for PS−F. However, for extruded nanocomposites this temperature was shifted to about 430 °C. At this temperature the char content was 7%, 5%, 4%, and only 2% for CN−PS-15, CN/PEO−PS-15, CN-*g*-PEG−PS-15, and CN-*g*-PEG/PEO−PS-15 nanocomposites, respectively. The lowest char content for CN-*g*-PEG/PEO−PS nanocomposites indicates higher compatibility between CN-*g*-PEG/PEO nanofiller and PS matrix, which promote the integrated architecture of ensuing nanocomposites.

The mechanical properties of the four nanocomposite series were investigated by dynamic mechanical analysis (DMA). The evolution of the storage tensile modulus as a function of temperature was determined (results not shown). For the unfilled PS matrix a classical behavior for an amorphous

dx.doi.org/10.1021/ma4010154 | *Macromolecules* 2013, 46, 5570−5583

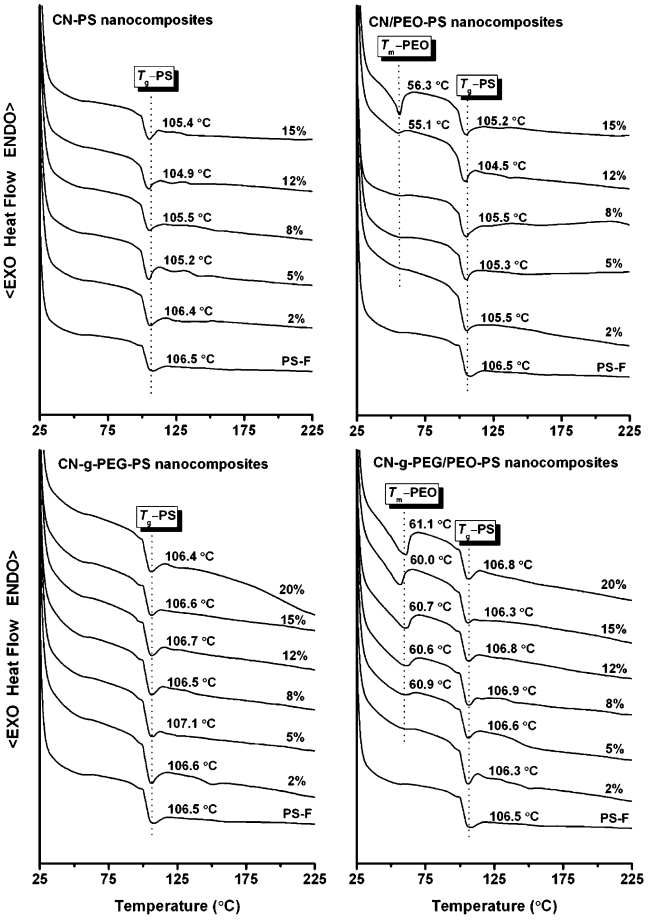

Figure 12. DSC thermograms for CN−PS, CN/PEO−PS, CN-*g*-PEG−PS, and CN-*g*-PEG/PEO−PS nanocomposites.

polymer was observed with two plateaus corresponding to the glassy and rubbery state of the polymer and a sharp modulus drop associated with the glass transition temperature (T_g). The glassy modulus of PS was not significantly affected when adding nanocrystals regardless their physical/chemical modification. This is attributed to the fact that in this temperature range the difference between the elastic modulus of CN and that of the glassy PS matrix was not high enough to easily appreciate a reinforcing effect for such low filler contents.[32] However, above T_g, the reinforcing effect of nanocrystals becomes apparent ($E_{CN} \gg E_{PS}$), and the modulus of nanocomposites was higher than neat PS material.

The evolution of the storage tensile modulus at T_g + 10 °C (389 K) as a function of nanocrystal content is plotted in Figure 14. For pristine CN (black symbols), a negligible improvement of the stiffness of the material was observed. This could be ascribed to the low thermal stability of this series which resulted in nanocomposites reinforced with degraded CN. However, the maintenance of the storage modulus for CN−PS nanocomposites indicates the possible incomplete thermal degradation of nanocrystals during processing at 200 °C. For nanocomposites filled with CN/PEO (red symbols), the modulus first slightly increased upon nanofiller addition, and suddenly dropped for CN/PEO contents higher than 10 wt %. Even if the thermal degradation of the nanofiller is limited by adsorbed PEO, this coating restricts the interactions between nanoparticles and then weaken the possible formation of a percolating cellulose network within the polymeric matrix. Moreover, indirect interactions between the nanoparticles are expected to establish through a soft melt PEO interphase. Interestingly, the PEG-grafted CN (CN-*g*-PEG and CN-*g*-PEG/PEO nanofillers) provided a higher reinforcing effect to the PS matrix even if it was reported that the chemical modification on polysaccharide nanocrystals induces the partial destruction of three-dimensional network of nanoparticles, which was unfavorable to the enhancement of mechanical properties.[33] As shown in Figure 14, below the percolation threshold (w_{Rc} = 7.49 wt %, calculated from the critical volume fraction (v_{Rc}) of the rigid phase at the percolation threshold),[34] the modulus of nanocomposites enhanced gradually. This is obviously ascribed to higher thermal stability and better dispersion within the polymeric matrix of grafted CN. It could also indicate that chemical grafting did not consume all hydroxyl groups on the surface of nanocrystals, which ensured the formation of weak hydrogen bonding between the nanocrystals. However, above the percolation threshold the modulus of CN-*g*-PEG−PS nanocomposites continued to gradually increase while it stabilized for CN-*g*-PEG/PEO−PS nanocomposites. It could be ascribed to adsorbed-PEO chains on the CN surface that may weaken the interactions among remaining free hydroxyl groups, and block the further nanocrystal network architecture.

Generally, the introduction of nanocellulose in a polymeric continuous phase improves the barrier performance of nanocomposites, because of the tortuous path induced to the diffusion and permeability of moisture or gas molecules.[35] The effect of adding CN, CN/PEO, CN-*g*-PEG, and CN-*g*-PEG/PEO nanohybrids on the water vapor permeation (WVP) for extruded nanocomposites is shown in Figure 15. With the addition of pristine CN, the WVP value increased remarkably by nearly three to six times compared to neat PS−F material. In fact, during the processing by extrusion at high temperature, pristine CN without any protection inevitably degraded and carbonized, which may leave interstices between nanoparticles and matrix for ensuing nanocomposites (as indicated in Figure 11 by SEM observation). These interstices provided the space and pathway for the travel of moisture, and ultimately deteriorated the water vapor barrier properties of CN−PS nanocomposites. When PEO-adsorbed nanocrystals CN/PEO were used, the possible interstices were filled with PEO chains, and it revived the nanobarrier effect of rigid nanocrystals, which can be proved by the decrease of WVP for nanocomposites containing low CN/PEO contents (<10 wt %). However, as mentioned before, the incompatibility and microphase separation between superfluous PEO (for 12 and 15 wt % nanofiller contents) and PS in nanocomposites caused the aggregation of hydrophilic PEO chains, which may promote the moisture sorption and increase WVP value again. A similar tendency was obtained for the WVP of CN-*g*-PEG−PS nanocomposites. As shown in Figure 15, the most promising nanocomposites based on their superior water vapor barrier properties were CN-*g*-PEG/PEO−PS materials, which commonly exhibited a reduction of 35% of WVP in comparison with neat PS−F. For CN-*g*-PEG/PEO−PS nanocomposites loaded with various nanofiller contents, the chemical grafting and physical adsorption on nanocrystals enhanced the thermal stability and facilitated the homogeneous dispersion and compatibility between modified nanocrystals and matrix. It should be pointed out that entanglements between grafted PEG chains and adsorbed PEO should inhibit the self-aggregation of

dx.doi.org/10.1021/ma4010154 | *Macromolecules* 2013, 46, 5570−5583

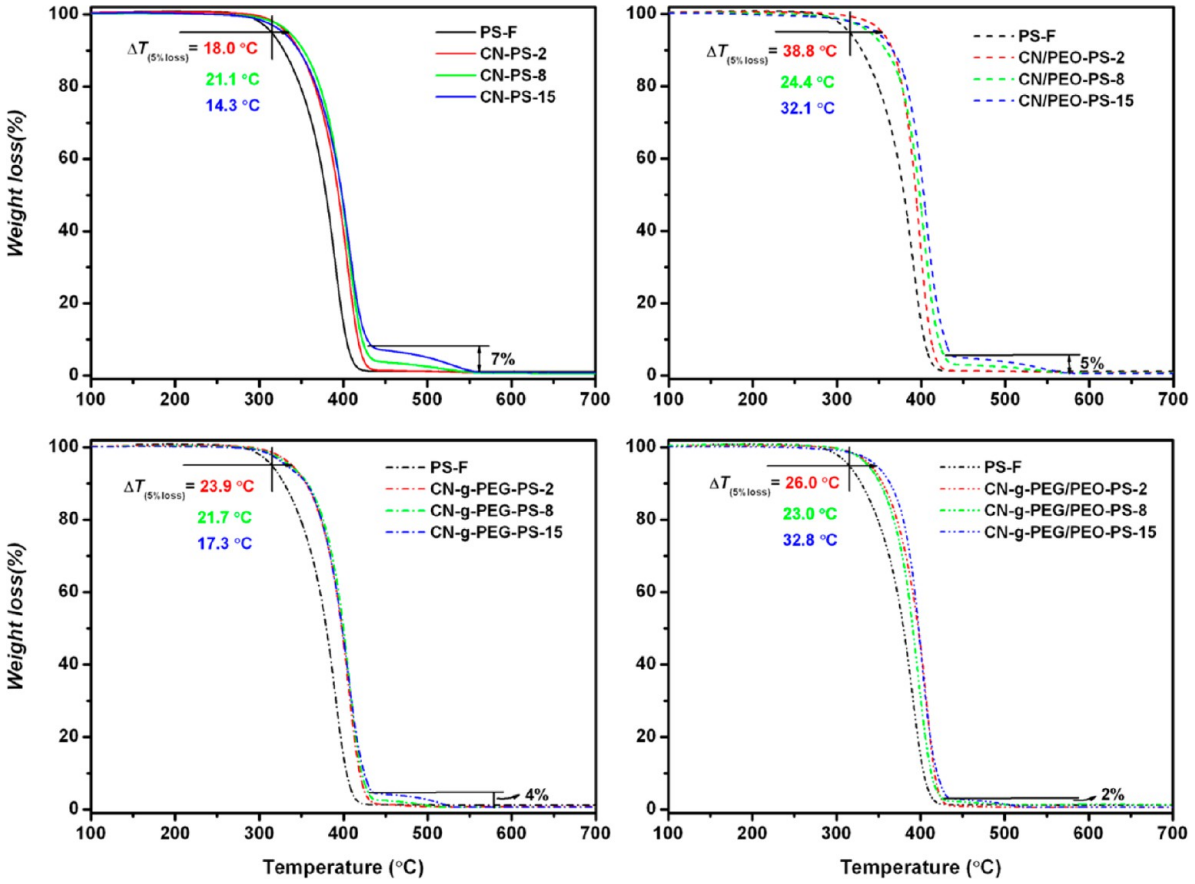

Figure 13. TGA for extruded nanocomposites with low (2 wt %), moderate (8 wt %), and high (15 wt %) nanohybrid contents.

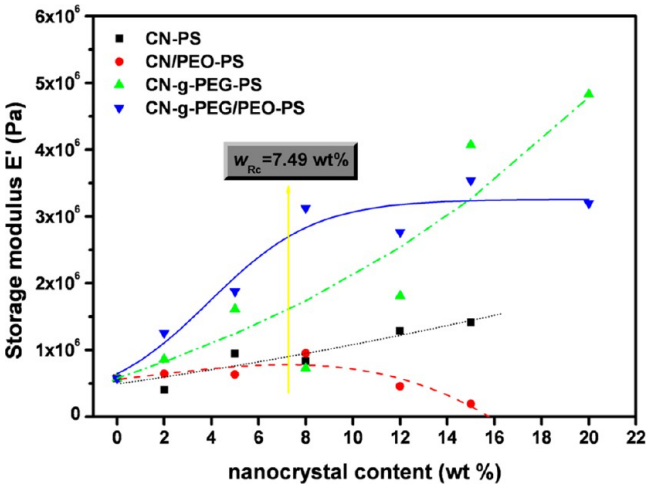

Figure 14. Storage modulus at T_g + 10 °C (389 K) and fitted curves for extruded nanocomposites vs nanocrystal content.

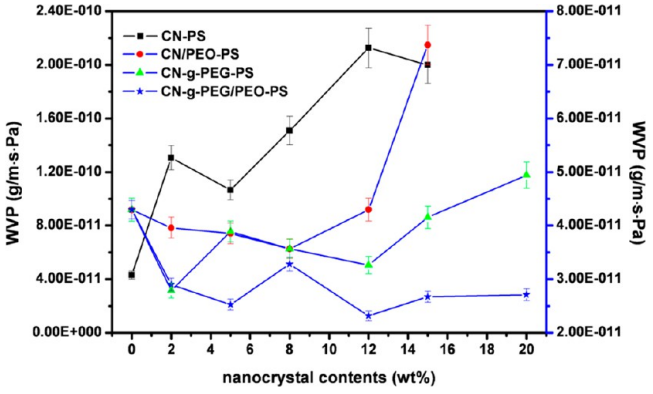

Figure 15. Effect of addition of CN, CN/PEO, CN-*g*-PEG, and CN-*g*-PEG/PEO nanohybrids on water vapor permeation (WVP) for extruded nanocomposites.

hydrophilic polymer; and at the same time long PEO chains served as "bridges" promoting the compatibility between modified nanocrystals and matrix. The well dispersed nanoparticles can create a tortuous pathway and block the effective travel for the diffusion of vapor through the composites matrix. Moreover, increased crystallinity of the PEO phase for CN-*g*-PEG/PEO−PS nanocomposites as shown from DSC analysis probably also facilitates this effect.

CONCLUSIONS

A strategy involving two poly(ethylene glycol)/polyoxyethylene (PEG/PEO) layers on the surface of cellulose nanocrystals using chemical grafting and physical adsorption was investigated. These modifications did not affect the crystallinity of the nanoparticles and improved their thermal stability. Four kinds of nanocrystals, i.e. pristine nanocrystal (CN), PEO-adsorbed nanocrystal (CN/PEO), PEG-grafted nanocrystal (CN-*g*-PEG), and both PEG-grafted and PEO-adsorbed nanocrystal (CN-*g*-PEG/PEO), were extruded with a hydrophobic polymeric matrix (PS) to prepare melt processed nanocomposites. The basic idea is

dx.doi.org/10.1021/ma4010154 | *Macromolecules* 2013, 46, 5570−5583

consistent with the possibility of entanglements and cocrystallization between short PEG chains and long PEO chains, which can closely wrap and protect the surface of the nanocrystals. Meanwhile, the chemical and physical compatibilization imparted by PEG and PEO layers promoted the interfacial interactions between cellulosic nanoparticles and apolar matrix. Preliminary results showed the possibility of processing modified nanocrystals (CN-*g*-PEG/PEO) at high temperature (200 °C) avoiding the degradation of the nanoparticle, and providing a good dispersion and compatibility between modified nanocrystals and matrix. Furthermore, the surface modifications of nanocrystals did not block totally the interactions between the nanoparticles, and kept at least partially the three-dimensional network architecture, which is beneficial for the improvement of mechanical and barrier properties of extruded nanocomposites. With this strategy, it is expected to overcome an important challenge aimed at melt processing nanocellulose based nanocomposites as industrial products. However, further investigation is necessary to fully understand the interactions between grafted PEG and adsorbed PEO, such as the chain length ratio (1/10 for PEG/PEO was used in this case), interphase thickness of PEG and PEO layers in extruded nanocomposites. Moreover, a simpler method for the introduction of the first PEG layer on cellulose nanocrystals to replace the chemical grafting reaction, such as electrostatic grafting, is another important issue to drive the practical application of this strategy. All these studies are in progress and will be present in future work.

■ ASSOCIATED CONTENT

Supporting Information

Results of composition for extruded nanocomposites in Table S1, data of XPS and elemental analysis in Table S2, and rheological analysis for CN-*g*-PEG/PEO (or CN/PEO) suspensions in Table S3. This material is available free of charge via the Internet at http://pubs.acs.org.

■ AUTHOR INFORMATION

Corresponding Author

*(A.D.) Telephone: +33 476826995. Fax: +33 476826933. E-mail: Alain.Dufresne@pagora.grenoble-inp.fr.

Notes

The authors declare no competing financial interest.

■ ACKNOWLEDGMENTS

The authors are grateful to Prof. Yun Chen (Wuhan University) for help on SEM observation, and Gregory Berthome (INPG-SIMaP) for help and discussion on XPS characterization. This work is supported by the China Scholarship Council (CSC) under Grant No. 2011695007.

■ REFERENCES

(1) Klemm, D.; Kramer, F.; Moritz, S.; Lindström, T.; Ankerfors, M.; Gray, D.; Dorris, A. *Angew. Chem., Int. Ed.* **2011**, *50*, 5438−5466.
(2) Habibi, Y.; Lucia, L. A.; Rojas, O. J. *Chem. Rev.* **2010**, *110*, 3479−3500.
(3) Moon, R. J.; Martini, A.; Nairn, J.; Simonsen, J.; Youngblood, J. *Chem. Soc. Rev.* **2011**, *40*, 3941−3994.
(4) Lin, N.; Huang, J.; Dufresne, A. *Nanoscale* **2012**, *4*, 3274−3294.
(5) Favier, V.; Canova, G. R.; Cavaillé, J. Y.; Chanzy, H.; Dufresne, A.; Gauthier, C. *Polym. Adv. Technol.* **1995**, *6*, 351−355.
(6) *The global market for nanocellulose to 2017*; Futures Markets Inc.: Canada, 2012, pp 1−66.
(7) Dagnon, K. L.; Shanmuganathan, K.; Weder, C.; Rowan, S. J. *Macromolecules* **2012**, *45*, 4707−4715.
(8) Fox, J. D.; Capadona, J. R.; Marasco, P. D.; Rowan, S. J. *J. Am. Chem. Soc.* **2013**, *135*, 5167−5174.
(9) Dufresne, A. *Nanocellulose. From nature to high performance tailored materials*; Walter de Gruyter GmbH: Berlin and Boston, MA; 2012, pp 252−260.
(10) Bellayer, S.; Gilman, J. W.; Eidelman, N.; Bourbigot, S.; Flambard, X.; Fox, D. M.; De Long, H. C.; Trulove, P. C. *Adv. Funct. Mater.* **2005**, *5*, 910−916.
(11) Alloin, F.; D'Aprea, A.; Dufresne, A.; El Kissi, N.; Bossard, F. *Cellulose* **2011**, *18*, 957−973.
(12) Orts, W. J.; Shey, J.; Imam, S. H.; Glenn, G. M.; Guttman, M. E.; Revol, J.-F. *J. Polym. Env.* **2005**, *13*, 301−306.
(13) Goffin, A.-L.; Raquez, J.-M.; Duquesne, E.; Siqueira, G.; Habibi, Y.; Dufresne, A.; Dubois, P. *Biomacromolecules* **2011**, *12*, 2456−2465.
(14) Goffin, A.-L.; Raquez, J.-M.; Duquesne, E.; Siqueira, G.; Habibi, Y.; Dufresne, A.; Dubois, P. *Polymer* **2011**, *52*, 1532−1538.
(15) de Menezes, A. J.; Siqueira, G.; Curvelo, A. A. S.; Dufresne, A. *Polymer* **2009**, *50*, 4552−4563.
(16) Raquez, J.-M.; Murena, Y.; Goffin, A.-L.; Habibi, Y.; Ruelle, B.; DeBuyl, F.; Dubois, P. *Compos. Sci. Technol.* **2012**, *72*, 544−549.
(17) Xu, S. H.; Gu, J.; Luo, Y. F.; Jia, D. M. *eXPRESS Polym. Lett.* **2012**, *6*, 14−25.
(18) Azouz, K. B.; Ramires, E. C.; Van den Fonteyne, W.; El Kissi, N.; Dufresne, A. *ACS Macro Lett.* **2012**, *1*, 236−240.
(19) Fortunati, E.; Armentano, I.; Zhou, Q.; Iannoni, A.; Saino, E.; Visai, L.; Berglund, L. A.; Kenny, J. M. *Carbohydr. Polym.* **2012**, *87*, 1596−1605.
(20) Zhou, Q.; Brumer, H.; Teeri, T. T. *Macromolecules* **2009**, *42*, 5430−5432.
(21) Oksman, K.; Mathew, A. P.; Bondeson, D.; Kvien, I. *Compos. Sci. Technol.* **2006**, *66*, 2776−2784.
(22) Bondeson, D.; Oksman, K. *Compos., Part A* **2007**, *38*, 2486−2492.
(23) Lin, N.; Chen, G.; Huang, J.; Dufresne, A.; Chang, P. R. *J. Appl. Polym. Sci.* **2009**, *113*, 3417−3425.
(24) Lin, N.; Bruzzese, C.; Dufresne, A. *ACS Appl. Mater. Interfaces* **2012**, *4*, 4948−4959.
(25) Montanari, S.; Roumani, M.; Heux, L.; Vignon, M. R. *Macromolecules* **2005**, *38*, 1665−1671.
(26) Habibi, Y.; Chanzy, H.; Vignon, M. R. *Cellulose* **2006**, *13*, 679−687.
(27) Araki, J.; Wada, M.; Kuga, S. *Langmuir* **2001**, *17*, 21−27.
(28) Follain, N.; Marais, M.-F.; Montanari, S.; Vignon, M. R. *Polymer* **2010**, *51*, 5332−5344.
(29) Thielemans, W.; Naceur Belgacem, M.; Dufresne, A. *Langmuir* **2006**, *22*, 4804−4810.
(30) Segal, L.; Creely, J. J.; Martin, A. E., Jr.; Conrad, C. M. *Text. Res. J.* **1959**, *29*, 786−794.
(31) Lin, N.; Huang, J.; Chang, P. R.; Feng, J.; Yu, J. *Carbohydr. Polym.* **2011**, *83*, 1834−1842.
(32) Loos, M. R.; Manas-Zloczower, I. *Polym. Eng. Sci.* **2013**, *53*, 882−887.
(33) Nair, K. G.; Dufresne, A. *Biomacromolecules* **2003**, *4*, 1835−1842.
(34) Dufresne, A.; Cavaille, J.-Y.; Helbert, W. *Polym. Compos.* **1997**, *18*, 198−210.
(35) Lavoine, N.; Desloges, I.; Dufresne, A.; Bras, J. *Carbohydr. Polym.* **2012**, *90*, 735−764.